An Analytic Five-Layer Quasigeostrophic Model for Initial-Value Problems

PAUL A. HIRSCHBERG* AND J. MICHAEL FRITSCH

Department of Meteorology, The Pennsylvania State University, University Park, Pennsylvania

(Manuscript received 26 November 1990, in final form 8 May 1991)

ABSTRACT

A five-layer analytic model of quasigeostrophic flow is developed. The model provides exact analytic solutions to the nonlinear quasigeostrophic omega and vorticity equations for various atmospheric temperature and geopotential structures. These solutions yield instantaneous three-dimensional fields of vertical motion and geopotential tendency given some finite-amplitude flow. Hence, unlike traditional eigenvalue analyses that provide time-dependent solutions for simple linearized flows, the five-layer model yields nonlinear diagnostic solutions to initial-value problems.

It is demonstrated that the five-layer model can reproduce many of the disturbance characteristics that are deduced from more traditional analyses of baroclinic instability. It is also shown that, because of its flexible vertical temperature structure specification, it can simulate complex temperature and geopotential structures in the atmosphere. The flexible specification of the total temperature and geopotential structure makes the five-layer model an attractive means for comparing theory with observations. Additionally, the versatility and simplicity of the five-layer model make it a potentially useful research and pedagogical tool.

1. Introduction

According to Petterssen and Smebye (1971), there are two different types of extratropical cyclogenesis. Systems that form in a manner resembling growth of a small perturbation on a baroclinically unstable basic state are termed Type A. Systems that occur when a preexisting upper-level disturbance interacts with a lower-tropospheric baroclinic zone are labeled Type B. Current theoretically based conceptualizations of Type B cyclogenesis proffer that low-level development results from the interaction between high- and low-level potential vorticity anomalies (e.g., Hoskins et al. 1985; Robinson 1989). A related view by Farrell (1982) (and supported by Rotunno and Fantini 1989) holds that Type B development can be considered as an initial-value problem. In this framework, Farrell (1982) showed that finite-amplitude disturbances can grow for physically significant time spans despite existing on linearly stable flows. Recent case studies of cyclone events generally support these conceptual models (e.g., Uccellini et al. 1987; Hirschberg and Fritsch 1991a,b).

Although linear stability analyses have clearly shown the sensitivity of Type A cyclone development to variations of the basic state, that is, static stability and wind shear of the background flow (e.g., Charney 1947; Eady 1949), it remains to be explored how sensitive Type B development (i.e., the initial-value problem) is to various configurations of upper- and lower-level features (e.g., potential vorticity anomalies). Investigative approaches compatible with the initial-value conceptual model have been taken by Sanders (1971, hereafter S), Farrell (1984), and Thorpe (1986). Sanders developed a one-layer model that provides analytic solutions of the nonlinear quasigeostrophic omega and vorticity equations for simple temperature, wind, and geopotential structures. The model yields instantaneous three-dimensional fields of vertical motion and geopotential height tendency given some finite-amplitude flow. Hence, unlike the more traditional eigenvalue analyses, which yield time-dependent solutions for simple linearized flows, the Sanders model yields nonlinear diagnostic solutions to initial-value problems.

The specification of the total temperature and geopotential structure makes the Sanders model an attractive means for comparing theory with observations. Observational studies have utilized modified versions of the model to compute the quasigeostrophic deepening rates and other quantities associated with cyclones (Bosart 1981; Sanders and Gyakum 1980; Gyakum 1983a,b). Although the Sanders model can simulate many of the gross characteristics of midlatitude baroclinic waves, its single-layer design limits its ability to represent certain aspects of the vertical structure of the atmosphere. More sophisticated versions of this model (e.g., Sanders and Gyakum 1980; Gyakum

* Present affiliation: Department of Meteorology, Naval Postgraduate School, Monterey, California.

Corresponding author address: Prof. Paul A. Hirschberg, Dept. of Meteorology, Naval Postgraduate School, Code MR/Hs, Monterey, CA 93943.

1983b) are also limited in this regard. The purpose of the present paper is to document an extension of the Sanders model to five layers and to present some brief results showing the efficacy of the new formulation for exploring initial-value sensitivities to vertical variations in static stability.

2. Five-layer model

The five-layer model extends the Sanders one-layer version by including:

1) five flexible-depth layers,
2) a vertically sloping temperature field,
3) a variable vertical static stability distribution in each layer,
4) a mean wind or meridional linear temperature gradient specification,
5) independent vertical distributions of the harmonic and linear components of the temperature field, and
6) a flexible reference geopotential specification.

Figure 1 depicts the vertical structure of the five-layer model. The horizontal fields are cyclic in the x and y directions, although a rectangular domain from $-L/2 \leq x \leq L/2$ and $-L/4 \leq y \leq -L/4$ (where L is the horizontal wavelength) is used for display purposes. The model is based on the specification of the model pressure levels P_j, the total three-dimensional temperature field $T(x, y, p)$, and the two-dimensional geopotential $\phi(x, y, P_j)$ [or geopotential height $z(x, y, P_j)$] field at one of the model levels. All other quantities (such as the geostrophic wind field) are derived from these fields.

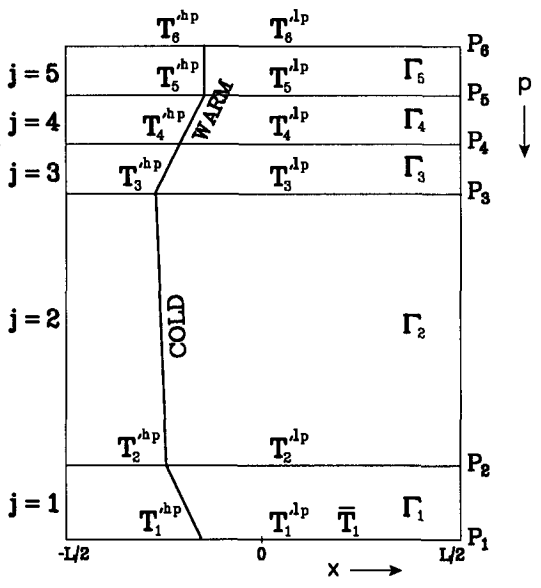

FIG. 1. A schematic cross section along $y = 0$ of the vertical structure of the five-layer model. Here $j = 1, \cdots, 5$ are the model layers; P_j, $j = 1, \cdots, 6$ are the model pressure levels; Γ_j, $j = 1, \cdots, 5$ are the mean lapse rates of temperature in each model layer j; $T_j'^{hp}$, $j = 1, \cdots, 6$ are the harmonic temperature amplitudes at each model level P_j; $-T_j'^{lp}$, $j = 1, \cdots, 6$ are the meridional temperature gradients at each model level P_j; and $\bar{T}_1$ is the mean temperature at P_1. The heavy solid line denotes the position of a representative axis of maximum absolute temperature deviation in the cross section.

a. Temperature

The temperature field consists of three components: a horizontal mean, a linear meridional gradient, and a harmonic component. The mean temperature structure is determined by specifying the average temperature at P_1 and the lapse rates in layers $j = 1, \cdots, 5$. The temperature deviation structure (meridional plus harmonic components) is found by specifying the meridional gradient and the harmonic amplitude at each model level (see Fig. 1). In addition, the phase lag of the harmonic component is set by specifying the location of the harmonic minimum, that is, the coldest air in the x direction at each model level. The function that prescribes the vertical structure of the temperature deviation field is similar to Sanders' function and is defined by

$$F_j(p) = A_j(1 - B_j \ln(p/P_j)). \tag{1}$$

The constants A_j and B_j are set so that the temperature deviations match at the layer interfaces. Consequently, the total temperature field is vertically continuous. Additionally, the damping function (1) for the linear and harmonic parts of the deviations can be set independent of one another, which enables a more flexible specification of the temperature field.

Schematically, the temperature field in layer j is expressed by

$$T_j(x, y, p) = \bar{T}_j(p) + T_j'^{l}(y, p) + T_j'^{h}(x, y, p), \tag{2}$$

where $\bar{T}_j(p)$ is the horizontal mean temperature, $T_j'^{l}(y, p)$ is the meridional component, and $T_j'^{h}(x, y, p)$ is the harmonic component. The mean temperature structure in each layer j can be expressed as

$$\bar{T}_j(p) = T_{0_j} p^{\beta_j}, \tag{3}$$

where

$$T_{0_j} = \bar{T}_j(P_j) P_j^{-\beta_j}, \tag{4}$$

and

$$\beta_j = \frac{\partial \ln \bar{T}_j}{\partial \ln p} = \frac{R}{g} \frac{\partial \bar{T}_j}{\partial z} = \frac{R}{g} \Gamma_j. \tag{5}$$

The linear meridional component of the temperature field in layer j is defined by

$$\begin{aligned} T_j'^{l}(y, p) &= -\epsilon_j{}^{l}(1 - \alpha_j{}^{l} \ln(p/P_j)) T_1'^{lp} y \\ &= -T_j'^{lp}(p) y, \end{aligned} \tag{6}$$

where $-T_1'^{lp}$ is the meridional temperature gradient at P_1, ${\alpha_j}^l$ determines the change of $T_j'^{lp}$ through layer j, and ${\epsilon_j}^l$ is a matching constant. Here ${\alpha_j}^l$ is given by

$$\alpha_j{}^l = f_j{}^l(\ln(P_{j+1}/P_j))^{-1}, \tag{7}$$

where $f_j{}^l$ is related to the ratio of the specified temperature gradient at level $j+1$ to that at level j. That is,

$$f_j{}^l = 1 - (T_j'^{lp}(P_{j+1})/T_j'^{lp}(P_j)). \tag{8}$$

The parameter ${\epsilon_j}^l$ is defined by the ratio of the meridional temperature gradient at level j to that at level $j=1$. Hence,

$$\epsilon_1{}^l = 1,$$

and

$$\begin{aligned}\epsilon_j{}^l &= (1 - \alpha_{j-1}^l \ln(P_j/P_{j-1}))\cdots(1 - \alpha_1{}^l \ln(P_2/P_1)) \\ &= T_j'^{lp}(P_j)/T_1'^{lp}, \quad j = 2, \cdots, 5.\end{aligned} \tag{9}$$

The harmonic temperature component of the temperature field in layer j is defined by

$$\begin{aligned}T_j'^h(x, y, p) &= -{\epsilon_j}^h(1 - {\alpha_j}^h \ln(p/P_j)) \\ &\times (T_1'^{hp}\cos(2\pi y/L)\cos[2\pi x/L + \lambda_j(p)]) \\ &= -T_j'^{hp}(p)\cos(2\pi y/L) \\ &\times \cos[2\pi x/L + \lambda_j(p)],\end{aligned} \tag{10}$$

where $T_1'^{hp}$ is the amplitude of the harmonic temperature component at P_1, ${\alpha_j}^h$ determines the change of $T_j'^{hp}$ through layer j, and ${\epsilon_j}^h$ is a matching constant. Here ${\alpha_j}^h$ and ${\epsilon_j}^h$ are defined similar to ${\alpha_j}^l$ and ${\epsilon_j}^l$ in (7) and (9) except that the harmonic temperature component values are used instead of the meridional component values. The phase of the harmonic temperature anomaly as a function of elevation in the x direction is given by

$$\lambda_j(p) = {\alpha_j}^p \ln(p/P_j) + \delta_j. \tag{11}$$

In this expression

$$\alpha_j{}^p = (2\pi/L)f_j{}^p(\ln(P_{j+1}/P_j))^{-1}, \tag{12}$$

where $f_j{}^p$ is some real fraction of L ($-f_j{}^p$ should be the desired location of the harmonic minimum at level $j+1$) and δ_j is the value of λ_j at the base of layer j.

b. Geopotential

The geopotential field is found by integrating the hypsometric equation

$$\phi(p) - \phi(p_b) = -R\int_{p_b}^{p} T(p)\,d\ln p, \tag{13}$$

where p_b is some pressure level where the geopotential ϕ is known. Upon substituting (2) into (13), the geopotential field in layer j can be partitioned into three parts, which correspond to each of the components of the temperature field, that is,

$$\phi_j(x, y, p) = \bar{\phi}_j(p) + \phi_j'^l(y, p) + \phi_j'^h(x, y, p). \tag{14}$$

The mean geopotential at P_1 is assumed to be zero so that $\bar{\phi}_1 = 0$. From (3) and (13), the mean geopotential in layer j is given by

$$\bar{\phi}_j(p) = \begin{cases} \bar{\phi}_j(P_j) - RT_{0_j}\ln(p/P_j), & \text{if } \beta_j = 0 \\ \bar{\phi}_j(P_j) - [(RT_{0_j})/\beta_j](p_j{}^{\beta_j} - P^{\beta_j}), & \text{if } \beta_j \neq 0. \end{cases} \tag{15}$$

To completely specify the three-dimensional geopotential deviation field, there must be one horizontal level P_{ref} at which the total (meridional and harmonic) geopotential deviation pattern is known. The two-dimensional geopotential deviation structure can be specified at any of the model levels $P_{\text{ref}} = P_j$ by the following expression

$$\begin{aligned}\phi'_{\text{ref}}(x, y, P_j) &= -\phi_{\text{ref}}'^{lp} y \\ &- \phi_{\text{ref}}'^{hp}\cos(2\pi x/L + \theta_{\text{ref}})\cos(2\pi y/L),\end{aligned} \tag{16}$$

where $-\phi_{\text{ref}}'^{lp}$ is the linear meridional geopotential gradient at P_{ref}, $\phi_{\text{ref}}'^{hp}$ is the harmonic geopotential amplitude at P_{ref}, and θ_{ref} is the phase in the x direction of the harmonic component of the geopotential field at P_{ref}. The phase θ_{ref} is given by

$$\theta_{\text{ref}} = (2\pi/L)f_{\text{ref}}^{\phi}, \tag{17}$$

where f_{ref}^{ϕ} is some real fraction of L ($-f_{\text{ref}}^{\phi}$ should be the desired location of the harmonic minimum at level P_{ref}). The mean zonal geostrophic wind at level P_{ref} is

$$U(P_{\text{ref}}) = -f_0{}^{-1}\left(\frac{\partial\phi_{\text{ref}}'^l}{\partial y}(x, y, P_{\text{ref}})\right) = \phi_{\text{ref}}'^{lp} f_0{}^{-1}. \tag{18}$$

Thus, the constant $\phi_{\text{ref}}'^{lp}$ can be set by specifying the mean geostrophic wind $U(P_{\text{ref}})$ at P_{ref}; that is,

$$\phi_{\text{ref}}'^{lp} = U(P_{\text{ref}})f_0. \tag{19}$$

Once the two-dimensional geopotential deviation field is specified at one model level $P_{\text{ref}} = P_j$, the geopotential patterns at the other model levels are found by integrating the hypsometric equation either up or down from the reference level. The continuous geopotential deviation field in each model layer j is found by integrating the hypsometric equation upward from the bottom level P_j of each layer. After some manipulation, the meridional component of the geopotential field in layer j can be expressed as

$$\begin{aligned}\phi_j'^l(y, p) &= \phi_j'^l(y, P_j) \\ &+ R{\epsilon_j}^l p_j'(1 - \alpha_j{}^l(p_j'/2))T_1'^{lp} y,\end{aligned} \tag{20}$$

where

$$p_j' = \ln(p/P_j), \tag{21}$$

and the harmonic component of the geopotential deviation as

$$\phi_j'^h(x, y, p) = (M_j \cos(x') + Q_j \sin(x')) \cos(y'), \tag{22}$$

where

$$M_j = M_j(p) = M_{j-1}(P_j) + m_j(p), \tag{23}$$

$$Q_j = Q_j(p) = Q_{j-1}(P_j) + q_j(p), \tag{24}$$

$$x' = 2\pi x/L,$$

$$y' = 2\pi y/L, \tag{25}$$

$$m_j = R\epsilon_j{}^h T_1'^{hp}[a_j \cos(\delta_j) + b_j \sin(\delta_j)], \tag{26}$$

$$q_j = R\epsilon_j{}^h T_1'^{hp}[b_j \cos(\delta_j) - a_j \sin(\delta_j)], \tag{27}$$

$$a_j = ((\alpha_j{}^p)^{-1} \sin(\alpha_j{}^p p_j') + (\alpha_j{}^h/(\alpha_j{}^p)^2) \times [1 - \cos(\alpha_j{}^p p_j')] - [(\alpha_j{}^h p_j')/\alpha_j{}^p] \sin(\alpha_j{}^p p_j')), \tag{28}$$

and

$$b_j = (-(\alpha_j{}^p)^{-1}[1 - \cos(\alpha_j{}^p p_j')] + (\alpha_j{}^h/(\alpha_j{}^p)^2) \times \sin(\alpha_j{}^p p_j') - [(\alpha_j{}^h p_j')/\alpha_j{}^p] \cos(\alpha_j{}^p p_j')). \tag{29}$$

c. Vertical motion

In each layer, the model flow is assumed to be governed by the inviscid quasigeostrophic vorticity equation

$$\frac{\partial \zeta_j}{\partial t} = -\mathbf{v}_j \cdot \nabla \eta_j + \eta_{0_j} \frac{\partial \omega_j}{\partial p}, \tag{30}$$

and by the adiabatic thermodynamic equation

$$\frac{\partial^2 \phi_j}{\partial t \partial p} = -\mathbf{v}_j \cdot \nabla \frac{\partial \phi_j}{\partial p} - \sigma_j(p)\omega_j, \tag{31}$$

where η_{0_j} is a constant value of the absolute geostrophic vorticity $\eta_j = \zeta_j + f$ in layer j. The quasigeostrophic stability parameter $\sigma_j(p)$ is defined as

$$\sigma_j(p) = \frac{R}{p} s_j(p) = \frac{\partial \phi_j}{\partial p} \frac{\partial \ln\theta_j}{\partial p} = \left(\frac{k}{p} - \frac{d \ln \bar{T}_j(p)}{dp}\right) \frac{R\bar{T}_{m_j}}{p} = [R\bar{T}_{m_j}\gamma_j]/p^2, \tag{32}$$

where $\bar{T}_{m_j}$ is a layer-average temperature,

$$k = R/c_p, \tag{33}$$

and

$$\gamma_j = k - \beta_j. \tag{34}$$

The quasigeostrophic omega equation,

$$\left(\nabla^2 + \frac{f_0\eta_{0_j}}{\sigma_j}\frac{\partial^2}{\partial p^2}\right)\omega_j = \frac{f_0}{\sigma_j}\left(\frac{\partial}{\partial p}(\mathbf{v}_j \cdot \nabla\eta_j)\right) - \frac{1}{\sigma_j}\left[\nabla^2\left(\mathbf{v}_j \cdot \nabla \frac{\partial \phi_j}{\partial p}\right)\right], \tag{35}$$

is used to deduce the three-dimensional field of vertical motion in each layer j. To solve this equation, it is first necessary to evaluate the forcing terms on the right side, that is, the differential vorticity advection and Laplacian of temperature advection. This tedious derivation (see Hirschberg 1989 for details) yields

$$\left(\nabla^2 + \frac{f_0\eta_{0_j}}{R\bar{T}_{m_j}\gamma_j} p^2 \frac{\partial^2}{\partial p^2}\right)\omega_j = (\Omega_j{}^s \sin(x') + \Omega_j{}^c \cos(x')) \cos(y') + \Omega_j{}^{2s} \sin(2y'). \tag{36}$$

In this expression

$$\Omega_j{}^s = \Omega_j{}^s(p) = \underset{1}{-f_j{}^{\omega 1} M_j p(1 - \alpha_j{}^l p_j')} \underset{2}{- f_j{}^{\omega 2} p(1 - \alpha_j{}^h p_j') \cos(\lambda_j)}, \tag{37}$$

$$\Omega_j{}^c = \Omega_j{}^c(p) = \underset{3}{f_j{}^{\omega 1} Q_j p(1 - \alpha_j{}^l p_j')} \underset{4}{- f_j{}^{\omega 2} p(1 - \alpha_j{}^h p_j') \sin(\lambda_j)}, \tag{38}$$

$$\Omega_j{}^{2s} = \Omega_j{}^{2s}(p) = \underset{5}{-f_j{}^{\omega 3} p(1 - \alpha_j{}^h p_j')(M_j \sin(\lambda_j) + Q_j \cos(\lambda_j))}, \tag{39}$$

where

$$f_j{}^{\omega 1} = \frac{4(2\pi/L)^3}{f_0\bar{T}_{m_j}\gamma_j} \epsilon_j{}^l T_1'^{lp}, \tag{40}$$

$$f_j{}^{\omega 2} = \frac{(2\pi/L)}{\bar{T}_{m_j}\gamma_j} \epsilon_j{}^h T_1'^{hp} \frac{\partial f}{\partial y}, \tag{41}$$

and

$$f_j{}^{\omega 3} = \frac{2(2\pi/L)^4}{f_0\bar{T}_{m_j}\gamma_j} \epsilon_j{}^h T_1'^{hp}. \tag{42}$$

As in S, it is informative to trace the physical identities of the forcing terms on the right side of (36). The five forcing terms are denoted underneath the expansions (37)–(39). Terms 1 and 3 are composed of two identical contributions: the vertical differential advection of that part of the relative vorticity field attributable to the harmonic temperature variation by that part of the wind

field due to the mean meridional temperature field $[\partial/\partial p(-\mathbf{v}_j{}^l \cdot \nabla \zeta_j{}^h)]$, and the Laplacian of the advection of the mean meridional temperature field by that part of the flow due to the harmonic temperature gradient $[\nabla^2(-\mathbf{v}_j{}^h \cdot \nabla T_j{}^l)]$. Terms 2 and 4 are due to the advection of the vorticity owing to the rotation of the earth by that part of the wind attributable to the harmonic temperature field $[\partial/\partial p(-\mathbf{v}_j{}^h \cdot \nabla f)]$. Finally, term 5 is due to the Laplacian of the advection of that part of the temperature field attributable to the harmonic temperature variation by that part of the flow also due to the harmonic temperature variation $[\nabla^2(-\mathbf{v}_j{}^h \cdot \nabla T_j{}^h)]$. It is not surprising to find, from a comparison of the forcing mechanisms in the original Sanders model (see S) and those described here for the five-layer model, that all of the mechanisms present in the Sanders model are also present in the five-layer model. It is significant to note, however, that there are forcing mechanisms in the five-layer model that are not present in the Sanders version. Specifically, part of term 5 in the five-layer model represents the advection of the harmonic component of the temperature field by the harmonic part of the thermal wind $(-\Delta \mathbf{v}_j{}^h \cdot \nabla T_j{}^h)$. This term is nonzero when there is a directional shear of the thermal wind within any layer j, which occurs in the model only if there is a vertical tilt in the harmonic temperature field with height; that is, if $\alpha_j{}^p \neq 0$. The contribution of this term to the total temperature advections can be significant. For example, a westward phase lag of $0.10L$ (290 km) between the 1000-mb and 500-mb harmonic temperature deviations for the model parameter set utilized by S results in an increase of the 500-mb temperature advection maximum from 7.17 K h^{-1} to 9.08 K h^{-1} or about 27%.

The solution to (36) is easier to obtain, following S, if the equation is separated into three parts such that each part corresponds to one of the three forcing functions on the right side of the equation. Consequently, ω_j is assumed to be composed of three distinct components such that

$$\omega_j(x, y, p) = \sum_{k=1}^{3} \omega_j{}^k(x, y, p), \tag{43}$$

where each $\omega_j{}^k(x, y, p)$ is a solution of

$$\left(\nabla^2 + \frac{f_0\eta_{0_j}}{R\bar{T}_{m_j}\gamma_j} p^2 \frac{\partial^2}{\partial p^2}\right) \omega_j{}^k(x, y, p) = F_j{}^{\omega k}(p) G^k(x, y). \tag{44}$$

In (44), $F_j{}^{\omega k}$ represents either $\Omega_j{}^s$, $\Omega_j{}^c$, or $\Omega_j{}^{2s}$, and $G^k(x, y)$ represents the kth harmonic function on the right side of (36). Since each of the $\omega_j{}^k(x, y, p)$ must vanish in the horizontal where its forcing function vanishes, that is, where $G^k(x, y) = 0$, the spatial dependencies in the omega equations can be eliminated (see Hirschberg 1989) and the three expressions reduced to the form

$$\left(p^2 \frac{d^2}{dp^2} - K_j{}^{-1}\right) \hat{\omega}_j{}^k(p) = H_j{}^{\omega k}(p) K_j{}^{-1} = I_j{}^{\omega k}(p), \tag{45}$$

where

$$H_j{}^{\omega k}(p) = [n(2\pi/L)^2]^{-1} F_j{}^{\omega k}(p), \tag{46}$$

$$K_j = \frac{f_{0_j}\eta_{0_j}}{2(2\pi/L)^2 R\bar{T}_{m_j}\gamma_j}, \tag{47}$$

and

$$n = \begin{cases} 2, & \text{if } k = 1 \text{ or } 2 \\ 1, & \text{if } k = 3. \end{cases} \tag{48}$$

The three omega equations represented by (45) have Euler forms that are more easily solved in terms of a new vertical coordinate Z, such that

$$Z = p_j' = \ln(p/P_j). \tag{49}$$

In terms of Z, the omega equations can be written as

$$\frac{d^2\hat{\omega}_j{}^k(Z)}{dZ^2} - \frac{d\hat{\omega}_j{}^k(Z)}{dZ} - b_j{}^k \hat{\omega}_j{}^k(Z) = I_j{}^{\omega k}(Z), \tag{50}$$

where $b_j{}^k$ is a constant and $I_j{}^{\omega k}(Z)$ are the transforms of $I_j{}^{\omega k}(p)$. Now, the equations represented by (50) are linear and have solutions that consist of homogeneous and particular parts. The homogeneous equations have general solutions of the form

$$\hat{\omega}_j{}^{kh}(Z) = C_j{}^{k1} \exp(r_j{}^{k1} Z) + C_j{}^{k2} \exp(r_j{}^{k2} Z), \tag{51}$$

where $C_j{}^{k1}$ and $C_j{}^{k2}$ are constants to be determined,

$$r_j{}^{k1} = \frac{1}{2} + \frac{1}{2}(1 + 4b_j{}^k)^{1/2}, \tag{52}$$

$$r_j{}^{k2} = \frac{1}{2} - \frac{1}{2}(1 + 4b_j{}^k)^{1/2}, \tag{53}$$

and

$$b_j{}^k = \begin{cases} K_j{}^{-1}, & \text{if } k = 1 \text{ or } 2 \\ 2K_j{}^{-1}, & \text{if } k = 3. \end{cases} \tag{54}$$

The particular solutions of the model omega equations can be found by applying the method of undetermined coefficients. This technique is based on the deduction of the functional form of the particular solution. In general, the deduced function will include some number of unknown coefficients whose values must be subsequently determined in order for the function to satisfy the differential equation. This determination is made by substituting the function into the differential equation and solving for the unknown coefficients (Kreyszig 1972). Fortunately, the three model omega equations have solution forms that are easily deduced. These are

$$\hat{\omega}_j^{ip}(Z) = W_j^{i1}Z^2\exp(Z)\cos(\lambda_j) + W_j^{i2}Z^2\exp(Z)\sin(\lambda_j) + W_j^{i3}Z\exp(Z)\cos(\lambda_j) + W_j^{i4}Z\exp(Z)\sin(\lambda_j) + W_j^{i5}\exp(Z)\cos(\lambda_j) + W_j^{i6}\exp(Z)\sin(\lambda_j) + W_j^{i7}Z\exp(Z) + W_j^{i8}\exp(Z), \quad (55)$$

for $i = 1$ and 2; and

$$\hat{\omega}_j^{3p}(Z) = W_j^{31}Z\exp(Z)\cos(\alpha_j^p Z) + W_j^{32}Z\exp(Z)\sin(\alpha_j^p Z) + W_j^{33}\exp(Z)\cos(\alpha_j^p Z) + W_j^{34}\exp(Z)\sin(\alpha_j^p Z) + W_j^{35}Z^2\exp(Z) + W_j^{36}Z\exp(Z) + W_j^{37}\exp(Z), \quad (56)$$

where the W_j^{kq} are the constants to be obtained. Upon substituting (55) and (56) into (50) with $k = 1$, 2, and 3, respectively, and equating coefficients, three sets of simultaneous linear equations for each layer j emerge that must be solved in order to determine the unknown coefficients W_j^{kq}. The solutions of these three sets of equations can be obtained straightforwardly with Cramer's rule or with the aid of a symbolic manipulator. The resulting complicated expressions are long and are therefore not presented here (see Hirschberg 1989 for details).

The particular solutions $\hat{\omega}_j^{kp}(Z)$ are fully determined once the coefficients W_j^{kq} are found. Thereafter, the general solutions $\hat{\omega}_j^{k}(Z)$ are obtained by adding the particular solutions to the appropriate homogeneous solutions (51). Expression of these solutions in terms of p yields the general solutions of the three-component omega equations for layer j. These are

$$\hat{\omega}_j^{1}(p) = C_j^{11}(p/P_j)^{r_j^{11}} + C_j^{12}(p/P_j)^{r_j^{12}} + (W_j^{11}p_j'^2 + W_j^{13}p_j' + W_j^{15})(p/P_j)\cos(\lambda_j) + (W_j^{12}p_j'^2 + W_j^{14}p_j' + W_j^{16})(p/P_j)\sin(\lambda_j) + (W_j^{17}p_j' + W_j^{18})(p/P_j), \quad (57)$$

$$\hat{\omega}_j^{2}(p) = C_j^{21}(p/P_j)^{r_j^{21}} + C_j^{22}(p/P_j)^{r_j^{22}} + (W_j^{21}p_j'^2 + W_j^{23}p_j' + W_j^{25})(p/P_j)\cos(\lambda_j) + (W_j^{22}p_j'^2 + W_j^{24}p_j' + W_j^{26})(p/P_j)\sin(\lambda_j) + (W_j^{27}p_j' + W_j^{28})(p/P_j), \quad (58)$$

and

$$\hat{\omega}_j^{3}(p) = C_j^{31}(p/P_j)^{r_j^{31}} + C_j^{32}(p/P_j)^{r_j^{32}} + (W_j^{31}p_j' + W_j^{33})(p/P_j)\cos(\alpha_j^p p_j') + (W_j^{32}p_j' + W_j^{34})(p/P_j)\sin(\alpha_j^p p_j') + (W_j^{35}p_j'^2 + W_j^{36}p_j' + W_j^{37})(p/P_j). \quad (59)$$

The constants C_j^{k1} and C_j^{k2}, and hence the unique solutions of the total model omega equation, are found by applying boundary conditions to the general solutions (57)–(59). Since the model contains five layers, 10 such boundary conditions must be specified and applied simultaneously. Two of the conditions are that the vertical motion vanishes at the top and bottom boundaries of the model. These conditions imply

$$\hat{\omega}_5^{k}(P_6) = 0, \quad k = 1, 2, \text{ and } 3, \quad (60)$$

and

$$\hat{\omega}_1^{k}(P_1) = 0, \quad k = 1, 2, \text{ and } 3, \quad (61)$$

where it is assumed that each omega component k must satisfy the boundary conditions separately. In some cases, it is more reasonable to demand that the vertical motion vanish at $p = 0$ mb. Thus, as an alternative to (60), the top boundary condition can be that

$$\hat{\omega}_5^{k}(0) = 0, \quad k = 1, 2, \text{ and } 3. \quad (62)$$

The other eight boundary conditions are that each omega amplitude $\hat{\omega}_j^{k}(p)$ and its first derivative must match at the layer interfaces. Hence,

$$\hat{\omega}_j^{k}(P_j) = \hat{\omega}_{j-1}^{k}(P_j), \quad j = 2, \cdots, 5, \quad (63)$$

and

$$\frac{d\hat{\omega}_j^{k}(P_j)}{dp} = \frac{d\hat{\omega}_{j-1}^{k}(P_j)}{dp}, \quad j = 2, \cdots, 5. \quad (64)$$

The latter condition ensures that the horizontal divergence is continuous across the isobaric layer interfaces.

Application of the boundary conditions (60)–(64) to the general model omega solutions (57)–(59) yield three sets of 10 simultaneous equations for the constants C_j^{k1} and C_j^{k2}. The exact form of the algebraic solutions of these equations can be obtained either manually or with the aid of a symbolic manipulator. The results, however, were found to be extremely complicated and cumbersome to analyze; thus, they are not presented here. Furthermore, the lengths of the solutions present formidable problems for computer applications. Consequently, an alternative method of obtaining the solutions is to numerically invert the matrix equations for any given specification of the model parameter values. Once the values of the constants C_j^{k1} and C_j^{k2} are known, the exact form of the model omega fields are fully determined.

d. Geopotential tendency

Evaluation of the geostrophic vorticity equation (31) provides the most straightforward means of obtaining the three-dimensional fields of geopotential tendency. With the aid of the geostrophic relationship, the vorticity equation can be written in terms of the geopotential tendency $\chi = \partial\phi/\partial t$. The result for layer j is

$$f_0 \frac{\partial \zeta_j}{\partial t} = \frac{\partial \nabla^2 \phi_j}{\partial t} = \nabla^2 \left(\frac{\partial \phi_j}{\partial t} \right) = \nabla^2 \chi_j$$

$$= -f_0 \mathbf{v}_j \cdot \nabla \eta_j + f_0 \eta_{0j} \frac{\partial \omega_j}{\partial p}. \quad (65)$$

From an inspection of the model expressions for the absolute vorticity advection (not presented) and the vertical motion, it is apparent that the forcing terms on the right side of (65) and the forcing terms on the right side of the model omega equation (36) share equivalent horizontal dependencies. As was the case for the omega equation, the solution of (65) is easier to obtain if it is separated into parts such that each part corresponds to one of the three horizontal functions on the right side of the equation. Therefore, similarly to ω_j, χ_j is assumed to be composed of three distinct components such that

$$\chi_j(x, y, p) = \sum_{k=1}^{3} \chi_j^k(x, y, p), \quad (66)$$

where each $\chi_j^k(x, y, p)$ is a solution of

$$\nabla^2 \chi_j^k(x, y, p) = L_j^{xk}(p) G^k(x, y). \quad (67)$$

In (67), $L_j^{xk}(p)$ is a function of a combination of the vorticity advection and the convergence amplitudes. Because each of the $\chi_j^k(x, y, p)$ must vanish in the horizontal where its respective forcing function vanishes, the spatial dependencies in the geopotential tendency equations can be eliminated and the three expressions for $\hat{\chi}_j^k$ reduced to

$$\hat{\chi}_j^k = -L_j^{xk}(p)[n(2\pi/L)^2]^{-1}$$

$$= f_0(\hat{V}_j^k + \eta_{0j} \hat{D}_j^k)[n(2\pi/L)^2]^{-1}, \quad (68)$$

where

$$n = \begin{cases} 2, & \text{if } k = 1 \text{ or } 2 \\ 4, & \text{if } k = 3, \end{cases} \quad (69)$$

the $\hat{D}_j^k$ are the amplitudes of the divergence $(-d\hat{\omega}_j^k/dp)$, and the $\hat{V}_j^k$ are the amplitudes of the negative absolute vorticity advections $(\mathbf{v}_j \cdot \nabla \eta_j)$ in layer j.

3. Model efficacy

a. Comparison with observations

In order to demonstrate the ability of the extended model to reproduce observed atmospheric structures, a few examples have been selected. First, a representative 200-mb level is shown because it typically intersects the tropopause and displays large horizontal variations in temperature, wind, and potential vorticity. Specifically, Fig. 2a shows an observed 200-mb height and temperature deviation (actual field minus map mean) pattern taken from the cyclone case study of Hirschberg and Fritsch (1991a,b). Note the large values

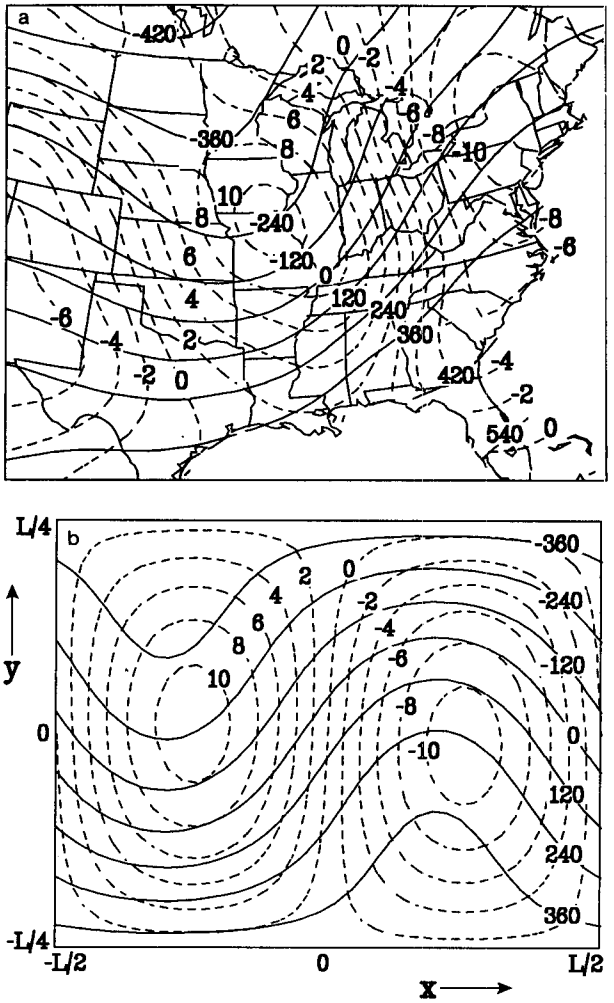

FIG. 2. (a) Analysis of a 200-mb height (solid, m) and temperature deviation (dashed, K) pattern taken for 1200 UTC 4 January 1982 (see Hirschberg and Fritsch 1991a,b); and (b) 200-mb height (solid, m) and temperature deviation pattern (dashed, K) taken from the five-layer model for conditions similar to those for the observed case in (a).

of the temperature deviations and crossing angles between the flow and the isotherms indicating that significant thermal advection is occurring between the trough and ridge axes. The pattern generated by the extended model (Fig. 2b) reproduces the main elements of the observed pattern.

The second example demonstrates the flexibility of the model in reproducing important vertical variations in the thermal field. In particular, Fig. 3a shows a cross section of an observed temperature deviation structure typical of a developing cyclone situation (Palmén and Newton 1969; Hirschberg and Fritsch 1991a). Contrary to the profiles of temperature perturbation derived from many linear models, which often decrease with elevation (e.g., Staley and Gall 1977), notice that the temperature deviations are large near 1000 mb, near

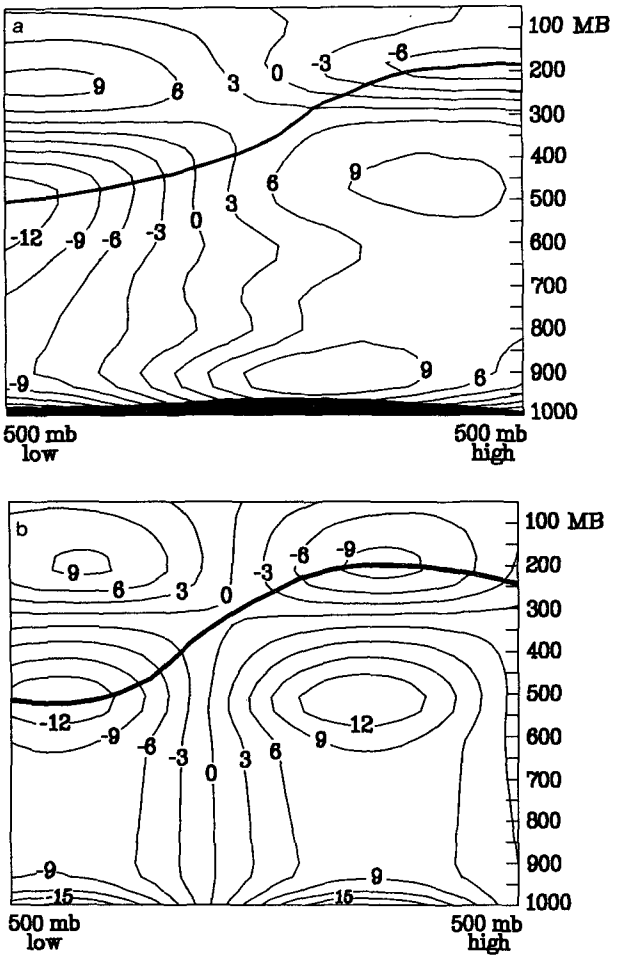

FIG. 3. (a) A cross section of an observed temperature deviation pattern (K) taken from the geographic center of a 500-mb low to the downstream center of a 500-mb high; see Hirschberg and Fritsch (1991a,b). The position of the tropopause (isentropic potential vorticity value of 10^{-6} m^2 s^{-1} K kg^{-1}) is denoted by a heavy solid line. (b) Cross section of temperature deviation (K) taken from the five-layer model for conditions similar to those for the observed cross section in (a). The model cross section is taken from the center of the model 500-mb low to the downstream center of the 500-mb high. The position of the model tropopause (along the axis of largest negative temperature perturbation) is denoted by a heavy solid line.

450 mb, and in the opposite sense near 200 mb. Note also how the deviations above 500 mb tilt slightly with elevation. Although this type of temperature structure cannot be adequately represented with a one-layer model, it can be simulated with the five-layer extended model, which permits tilt in the temperature field.

Figure 3b shows the model-generated structure that corresponds to the observed cross section. Clearly, the extended model is able to capture the main features of the observed thermal field. In addition to the upper-level deviations above 500 mb, lower-tropospheric temperature deviations are also present in the observed and model cross sections (Fig. 3) and are confined to a layer between 1000 and 800 mb. This layer can be considered the planetary boundary layer (PBL) in this example. Furthermore, the reversal of the signs of the temperature deviations above 500 mb often implicitly reveals the location of the tropopause. The observed cross section of Fig. 3a shows the typical case of a strong correlation between the tropopause location and the location of the axis of coldest temperature deviation above 500 mb. Likewise, although the tropopause is not explicitly represented in the five-layer model, the location of the tropopause can be inferred from the model cross section (Fig. 3b). With the extended model, the depth and other properties of the PBL, deep troposphere and stratosphere can easily be varied to test the impact on development. Such analyses and a more thorough discussion of the dynamics associated with the temperature structures described above as illuminated by the five-layer model will be presented in future papers.

The final example addresses the vertical variation of static stability. As indicated in section 2, the static stability parameterization $s(p)$ can be varied from layer to layer by assigning a mean temperature and lapse rate to each layer. The layer-mean values are dependent on the observed or hypothesized mean temperature distribution in the particular region of the atmosphere being defined. Figure 4 compares an observed vertical variation of $s(p)$ to that produced from a one-layer model and the five-layer model. As expected, the five-layer model is able to represent the observed distribution of static stability more faithfully than can a single-layer model. It is particularly noteworthy that it captures the stability change between the PBL, the deep troposphere, and the stratosphere.

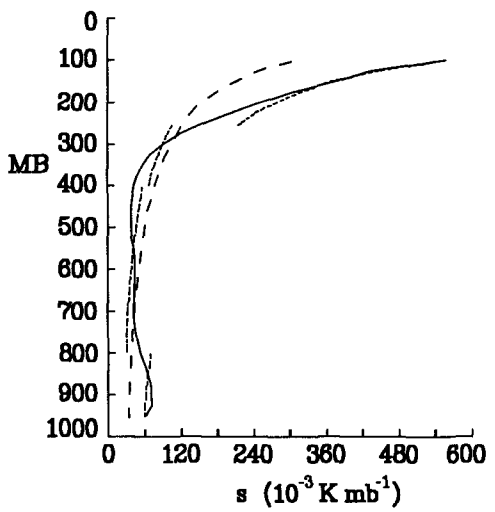

FIG. 4. Vertical profile of static stability $s = -T/\theta(\partial\theta/\partial p)$ (10^{-3} K mb^{-1}) from an observed case (solid) [see Hirschberg and Fritsch (1991a,b)], from the Sanders one-layer model (dashed), and from the five-layer model (short dashed).

b. Comparison with traditional results

As a simple check on the reliability of the five-layer model, its parameters were set such that the five layers collapsed into one and the results compared to the Sanders one-layer model. Figure 5 displays isopleths of the geopotential tendency χ_l of the five-layer model at the center of the 1000-mb cyclone as a function of wavelength L and 1000-mb meridional temperature gradient $T_y = T'^{lp}_1$. The tendencies are for a representative set of model parameter values utilized by S and for selected values of a vorticity–stability parameter defined by S as $VS = \eta_0/(T_0\gamma)$. Note that this stability parameter increases as the static stability decreases, and that the meridional temperature gradient T'^{l} varies in the vertical as $-T_y[1 - 0.722 \ln(1000/p)]$ (see S for details). Comparison of the results presented in Fig. 5 to those from S (his Fig. 13) shows them to be identical. It is evident that the characteristics of χ_l deduced from Fig. 5 are similar to various growth rate characteristics deduced from the stability diagrams of traditional eigenvalue models (e.g., Holton 1979) if χ_l is taken to be a relative measure of the instability of the baroclinic system simulated by the five-layer model. For instance, the primary region of instability lies between 1500 and 3500 km; the deepening rates increase with vertical wind shear ($T_y \propto \partial v/\partial p$) and with decreasing static stability (increasing VS); and the wavelength of maximum instability increases with wind shear and with increasing static stability (decreasing VS). Finally, there is a long-wave cutoff associated with the stabilizing β effect but no short-wave limit to the instability, a characteristic shared by other continuous models (Kuo 1952; Fleagle 1955; Green 1960). The dramatic change of the long-wave cutoff in the direction of more deepening as the VS increases is due to the inadequately weak stratospheric stability parameterization in the one-layer model.

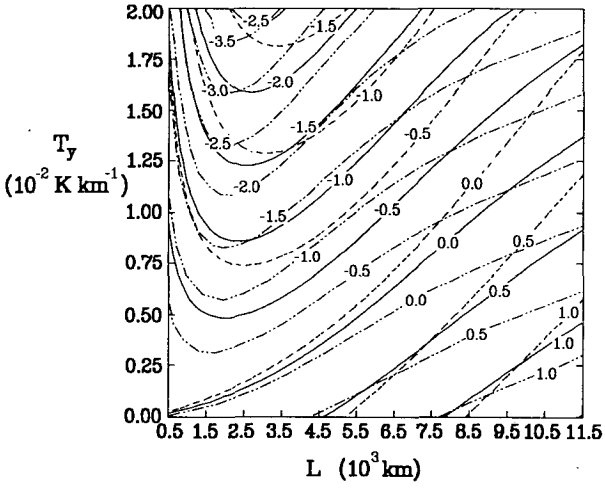

FIG. 5. Five-layer model deepening rate χ_1 (10^{-3} m^2 s^{-3}) at the 1000-mb low center as a function of horizontal wavelength L (10^3 km) and 1000-mb meridional temperature gradient T_y (10^{-2} K km^{-1}) for selected values of the vorticity–stability parameter $VS = \eta_0/(T_0\gamma)$. The dashed, solid, and dash–double-dot lines respectively are for values of $VS = 1.4 \times 10^{-6}$ K^{-1} s^{-1}, $VS = 2.8 \times 10^{-6}$ K^{-1} s^{-1}, and $VS = 5.6 \times 10^{-6}$ K^{-1} s^{-1}.

c. Some effects of enhanced vertical resolution

An examination of the sensitivity of χ_l to vertical variations of the mean lapse rate was made with the five-layer model. The relative value of the mean lapse rate Γ_j in each layer is negatively correlated with the static stability σ_j. Figure 6 shows the results of the sensitivity experiment. In the figure, isopleths of χ_l are plotted as functions of L and T_y for three configurations of Γ_j. The solid isopleths show the functional dependence of χ_l when a constant tropospheric lapse rate of 6.5 K km^{-1} is fixed throughout the depth of the model. The dashed lines are isopleths of the deepening rates when the lapse rate is raised to 9.0 K km^{-1} below 700 mb. Comparison of the solid and dashed isopleths shows that, when the lapse rate is increased (static stability decreased) in the lower part of the model, the deepening rates increase as a function of L and T_y over all wavelengths. The deepening rates of the shorter wavelengths (<4500 km) increase dramatically. In addition, the wavelength of maximum deepening decreases significantly.

The dash-double-dot lines in Fig. 6 are isopleths of deepening rates when the lapse rate is lowered to 0 K km^{-1} above 300 mb and held at 6.5 K km^{-1} below 300 mb. This simulates the addition of a stratospheric stable environment above typical tropospheric stability conditions. The addition of the high-level stable layer strongly suppresses the growth of longer wavelengths (>4000 km) but there is little change for shorter wavelengths. Furthermore, there is no shift in the wavelength of maximum deepening.

Although an exact, quantitative comparison between the results of this cursory experiment and the results of other (linear) models will not be attempted here, it is apparent that the deepening rate characteristics of the five-layer model are qualitatively similar to some of the results presented by other investigators. Staley and Gall (1977) found, for instance, that the short-wave end of their growth-rate spectrum was strongly destabilized by reducing the static stability in the lowest layer of their four-level model. They also found that the growth-rate spectrum was generally insensitive to upper-level static stability changes. Additionally, Blumen (1979) showed that short-wave instability was also sensitive to the relative depths and static stabilities in a two-layer Eady model.

4. Summary and conclusions

A five-layer analytic quasigeostrophic model that is based on the initial-value problem approach is developed. The model is an extension of a one-layer model formulated by Sanders (1971). It extends the Sanders

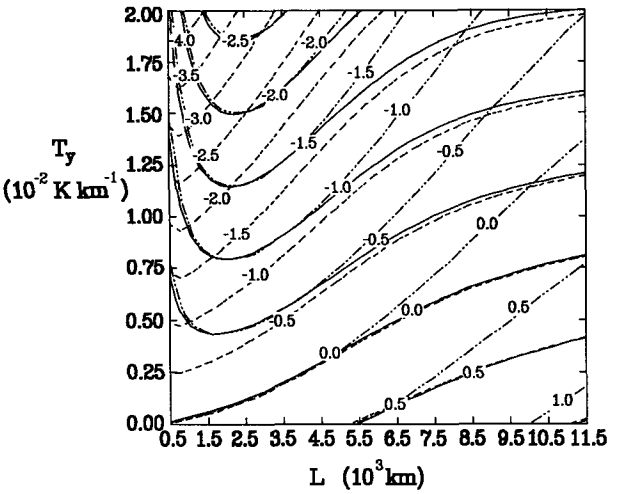

FIG. 6. Five-layer model deepening rate χ_1 (10^{-3} m^2 s^{-3}) as a function of horizontal wavelength L (10^3 km) and 1000-mb meridional temperature gradient T_y (10^{-2} K km^{-1}) and for three vertical configurations of Γ_j. The solid, dashed, and dash–double dot lines respectively are for values of Γ_j = constant = 6.5 K m^{-1} above 1000 mb; Γ_j = 9.0 K km^{-1} below 700 mb and Γ_j = 6.5 K km^{-1} above 700 mb; and Γ_j = 6.5 K km^{-1} below 300 mb and Γ_j = 0 K km^{-1} above 300 mb.

model by adding 1) five flexible-depth layers, 2) a vertically sloping temperature field, 3) a variable vertical static stability distribution in each layer, 4) a mean wind or meridional linear temperature-gradient specification, 5) independent vertical distributions of the harmonic and linear components of the temperature field, and 6) a flexible reference geopotential specification. The model yields analytic solutions to the nonlinear quasigeostrophic omega and vorticity equations for simple temperature and geopotential structures.

As demonstrated, the model can reproduce many of the results obtained from traditional eigenvalue studies of baroclinic instability. Additionally, the model was used to explore the more complicated effects of the initial-value sensitivities to vertical variations in static stability. In general, the simplicity of the model enables relatively straightforward experimentation and analysis. Since it can reproduce many of the complex initial atmospheric states observed in the midlatitudes, it can be a useful research and pedagogical tool for studying various quasigeostrophic phenomena and initial-value problems.

Acknowledgments. This work was supported by the National Science Foundation through Grants ATM-8521026 and ATM-8711014, by the Office of Naval Research through Grant SFRC No. N00014-86-K-0688, and by the Naval Postgraduate School in support of the Office of Naval Research "Heavy Weather at Sea" research initiative. Special thanks to Hampton N. Shirer for his assistance with the model development, to Peter R. Bannon, Toby N. Carlson, John H. E. Clark, Gregory S. Forbes, and Frederick Sanders for their helpful discussion and constructive suggestions, and to John R. Gyakum for his advice and for allowing us to inspect his model derivations.

REFERENCES

Blumen, W., 1979: On short-wave baroclinic instability. *J. Atmos. Sci.*, **36,** 1925–1933.

Bosart, L. F., 1981: The Presidents' Day snowstorm of 18–19 February 1979: A subsynoptic-scale event. *Mon. Wea. Rev.*, **109,** 1542–1566.

Charney, J. G., 1947: The dynamics of long waves in a baroclinic westerly current. *J. Meteor.*, **4,** 135–163.

Eady, E. T., 1949: Long waves and cyclone waves. *Tellus,* **1,** 33–52.

Farrell, B. F., 1982: The initial growth of disturbances in a baroclinic flow. *J. Atmos. Sci.*, **39,** 1663–1686.

——, 1984: Modal and non-modal baroclinic waves. *J. Atmos. Sci.*, **41,** 668–673.

Fleagle, R. G., 1955: Instability criteria and growth of baroclinic disturbances. *Tellus,* **7,** 168–176.

Green, J. S., 1960: A problem in baroclinic stability. *Quart. J. Roy. Meteor. Soc.*, **86,** 237–251.

Gyakum, J. R., 1983a: On the evolution of the QE II storm. I: Synoptic aspects. *Mon. Wea. Rev.*, **111,** 1137–1155.

——, 1983b: On the evolution of the *QE II* storm. II: Dynamic and thermodynamic structure. *Mon. Wea. Rev.*, **111,** 1156–1173.

Hirschberg, P. A., 1989: Tropopause undulations and the development of extratropical cyclones. Ph.D. thesis, The Pennsylvania State University, 633 pp. [Available from Dept. of Meteorology, Pennsylvania State University, University Park, PA 16802.]

——, and J. M. Fritsch, 1991a: Tropopause undulations and the development of extratropical cyclones: Part I. Overview and observations from a cyclone event. *Mon. Wea. Rev.*, **119,** 496–517.

——, and ——, 1991b: Tropopause undulations and the development of extratropical cyclones: Part II. Diagnostic analysis and conceptual model. *Mon. Wea. Rev.*, **119,** 518–550.

Holton, J. R., 1979: *An Introduction to Dynamic Meteorology.* Academic Press, 391 pp.

Hoskins, B. J., M. E. McIntyre and A. W. Robertson, 1985: On the use and significance of isentropic potential vorticity maps. *Quart. J. Roy. Meteor. Soc.*, **111,** 877–946.

Kreyszig, E., 1972: *Advanced Engineering Mathematics.* John Wiley and Sons, 866 pp.

Kuo, H. L., 1952: Three dimensional disturbances in a baroclinic zonal current. *J. Meteor.*, **9,** 260–278.

Palmen, E., and C. W. Newton, 1969: *Atmospheric Circulation Systems.* Academic Press, 603 pp.

Petterssen, S., and S. J. Smebye, 1971: On the development of extratropical cyclones. *Quart. J. Roy. Meteor. Soc.*, **97,** 457–482.

Robinson, W. A., 1989: On the structure of potential vorticity in baroclinic instability. *Tellus,* **41A,** 275–284.

Rotunno, R., and M. Fantini, 1989: Petterssen's "Type B" cyclogenesis in terms of discrete, neutral Eady modes. *J. Atmos. Sci.*, **46,** 3599–3604.

Sanders, F., 1971: Analytic solutions of the nonlinear omega and vorticity equations for a structurally simple model of disturbances in the baroclinic westerlies. *Mon. Wea. Rev.*, **99,** 393–408.

——, and J. R. Gyakum, 1980: Synoptic-dynamic climatology of the "bomb". *Mon. Wea. Rev.*, **108,** 1589–1606.

Staley, D. O., and R. L. Gall, 1977: On the wavelength of maximum baroclinic instability. *J. Atmos. Sci.*, **34,** 1679–1688.

Thorpe, A. J., 1986: Synoptic scale disturbances with circular symmetry. *Mon. Wea. Rev.*, **114,** 1384–1389.

Uccellini, L. W., R. A. Petersen, K. F. Brill, P. J. Kocin, and J. J. Tucillo, 1987: Synergistic interactions between an upper-level jet streak and diabatic processes that influence the development of a low-level jet and a secondary coastal cyclone. *Mon. Wea. Rev.*, **115,** 2227–2261.